J. Phys. Chem. Solids Vol. 53, No. 11, pp. 1473–1485, 1992
Printed in Great Britain.

0022-3697/92 $5.00 + 0.00

SUPERCONDUCTIVITY IN ALKALI INTERCALATED C_{60}

M. SCHLÜTER,† M. LANNOO,†‡ M. NEEDELS,† G. A. BARAFF† and D. TOMÁNEK§
†AT&T Bell Laboratories, Murray Hill, NJ 07974, U.S.A.
§Department of Physics and Astronomy, Michigan State University, East Lansing, MI 48824-1116, U.S.A.

(*Received* 4 *March* 1992)

Abstract—Superconductivity observed in alkali intercalated C_{60} solid can be explained on the basis of conventional BCS theory. Intra-molecular Jahn–Teller type vibrations with high frequencies couple to conduction electrons in C_{60} π-orbitals with strength V. The density of these states (N) is determined by the relatively weak intermolecular coupling. This results in a real space factorization of the coupling parameter $\lambda = NV$ which has several experimental consequences. We present detailed calculations that lead to this picture and compare with existing experiments.

Keywords: BCS, superconductivity, Jahn–Teller distortions.

1. INTRODUCTION

The discovery of superconductivity [1] in fcc alkali intercalated A_3C_{60} compounds (A = K, Rb, Cs) with T_c-values exceeding 30 K has created considerable excitement. The question arises whether superconductivity in these compounds can be explained in standard BCS terms using electron–phonon coupling or whether electron–correlation based couplings are operative. Also at issue is the appropriateness of BCS type coupling vs the condensation of strongly coupled, preformed bosons. Numerous models falling into these various categories have been proposed [2–11]. We here present the results of detailed studies of the electronic and vibronic properties of A_3C_{60} and their coupling to each other [3]. We find that standard BCS-type coupling to molecular vibrations can well account for all known observations. The uniqueness of the present situation arises from the particular molecular, chemical nature of the compounds rather than from unusual superconductivity mechanisms.

In section 2 we will discuss the basic electronic structure of A_3C_{60}, details relevant to superconductivity and a variety of approximations used to describe the electron states near the Fermi-level. In section 3 we will focus on the vibrational properties of A_3C_{60}, subdivide those into several groups of vibrations according to the nature of the molecule, and present numerical results for several models. In section 4 we study the electron-phonon coupling in detail and relate it to the Jahn–Teller coupling problem of an isolated C_{60} molecule. Finally, in section 5 we describe our results for superconductivity, including a discussion of Coulomb repulsion effects, the isotope effect, changes upon alkali substitution, effects of pressure, etc. We will compare with experiments where available and conclude in section 6 with a discussion of limiting circumstances for further enhancement of superconductivity in A_3C_{60}.

2. ELECTRONIC STATES IN A_3C_{60}

It is convenient to view the electronic structure of A_3C_{60} as a result of a stepwise refinement of energy scales. In this context we begin with the largest scale, that of an isolated C_{60} molecule. Each of the 60 atoms is three-fold coordinated at the vertex of two hexagons and one pentagon. There are a total of 12 pentagons, 20 hexagons and 90 bonds. While each atom is equivalent, the bonds are not: 60 (long) bonds exist separating pentagons and hexagons, while 30 (short) bonds separate hexagons. Experimentally [12, 13], the bond lengths are determined to be about 1.4 Å and 1.45 Å. The electronic structure of the isolated C_{60} molecule has been studied early by empirical methods [14]. The states can be classified into σ- and π-like revealing an insulating gap (1–2 eV) between the highest occupied, mostly π-like level (HOMO) and the lowest unoccupied mostly π^*-like level (LUMO). In the icosahedral group I_h, the HOMO is classified as a five-fold degenerate h_u level, while the LUMO is represented by a three-fold degenerate t_{1u} level. Both are part of a 11-fold degenerate $\ell = 5$ manifold of π-states (on a sphere) that is split by the iscosahedral symmetry of C_{60}. Since intercalation with alkali atoms will result in electron donation to C_{60}, the LUMO is of particular interest. Careful

‡ Permanent address: ISEN, Lille, France.

analysis shows that the phases of the three LUMO t_{1u}-states are bonding along the short bonds and antibonding along the long (pentagon) bonds. When placed into an fcc lattice with the measured lattice constant of $a_0 = a\sqrt{2} = 14.2$ Å, the closest carbon atoms of neighboring molecules are separated by $d \simeq 3.1$ Å, which is smaller than the interlayer separation in graphite (3.45 Å). While the electrons remain largely localized to the individual C_{60} molecules, small inter-molecular overlap exists.

The distribution of electronic charges is illustrated in Fig. 1 where the total valence electron density (top) is compared to the hypothetical charge of an electron added to the LUMO (bottom). The overlap between these LUMO states of two molecules is emphasized in Fig. 2. The calculations were done in the Density Functional (LDA) approach using a plane wave expansion and pseudopotentials yielding results in close agreement with other studies [15–19]. While the electronic structure of an isolated C_{60} is well understood, and near the gap given by the large intramolecular π–π hopping energy scale, details of the weak inter-molecular hopping and band formation are less well established. In particular, these details depend on the relative orientation of C_{60} molecules [20, 21], NMR [22, 23] and X-ray [24] experiments show that in pure, undoped C_{60} the molecules rotate freely at room temperature undergoing an ordering transition only below 260 K. At these temperatures the molecules still show correlated rotations which are only frozen out below ~ 140 K, as indicated by NMR studies [25]. Pulsed neutron studies show considerable orientational disorder to remain [26]. For intercalated material the structure is already frozen at room temperature [27]. The degree of order is not well established. The influence of molecular orientation on the electronic structure of the LUMO complex has recently been studied [20]. Ignoring details in the electronic structure (which would be washed out because of residual disorder) the main results of these studies are the formation of a ~ 0.5 eV wide LUMO band, separated from the next higher band by ~ 0.5 eV. The two energy scales of the ~ 10 eV wide π–π^* complex and the ~ 0.5 eV wide inter-molecular band dispersion are clearly separated, emphasizing the strong molecular nature of fcc C_{60}.

Solid C_{60}, intercalated with alkali atoms exhibits a rich phase diagram with both semiconducting and metallic phases [28]. We have concentrated on the (only) metallic phases of fcc A_3C_{60} or A_2BC_{60}. In

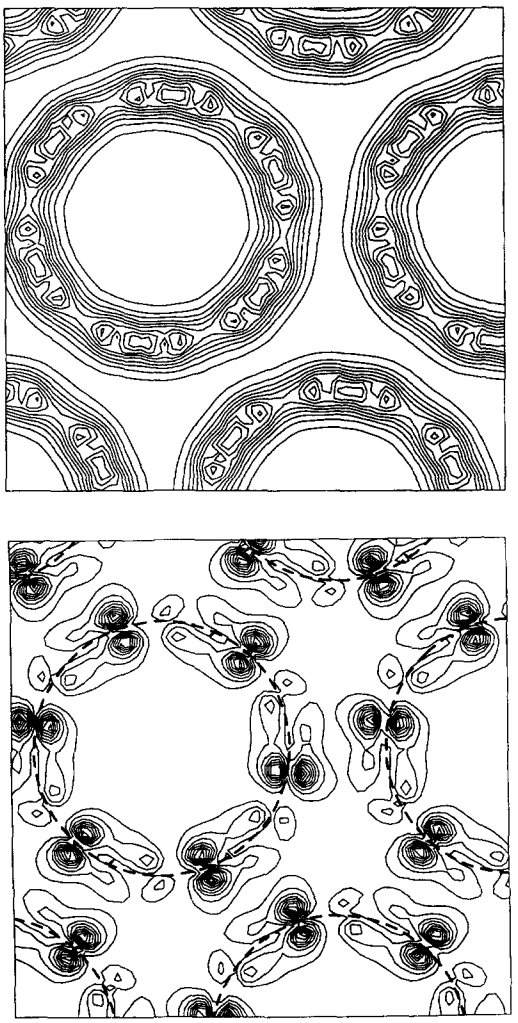

Fig. 1. Calculated electronic charge density contour plots of fcc C_{60}. The total valence charge density (top) is compared to the hypothetical charge density of an electron added to the LUMO (bottom). The densities are shown in a (111) plane intersecting the C_{60} molecules in an equatorial plane through bond, but not individual atoms. The calculations were done using pseudopotentials and plane waves.

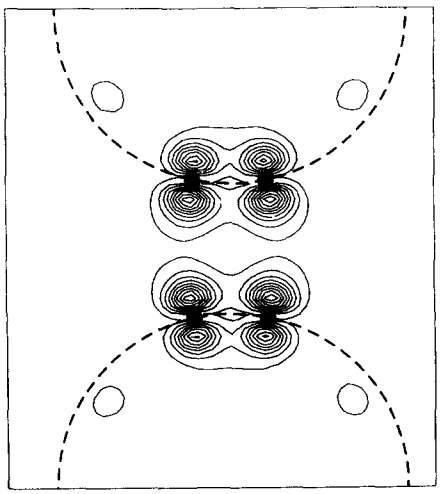

Fig. 2. Calculated charge density distribution of t_{1u} LUMO electrons, shown in a plane (close to (110)) containing two pairs of atoms on adjacent molecules. Overlap of this kind is responsible for the formation of a narrow conduction band in A_3C_{60}.

these phases alkali atoms occupy the two tetrahedral (A) and the one octahedral (B) interstitials. The C_{60} molecules are thought to be in their 'standard' T_h^3 configurations, with hexagons pointing in the (111) directions. There are two such orientations which presumably remain disordered. The key question regarding the electronic structure of A_3C_{60} is whether the alkali atoms merely act as donors of electrons into the mostly rigid C_{60} LUMO complex, or whether significant hybridization with these states takes place. Several independent calculations [3, 20, 30] show that the rigid band donor picture is essentially correct. The first alkali derived states are found ~ 2 eV above the t_{1u} LUMO band. The states near E_F in A_3C_{60} have then the approximate spatial distribution shown in Fig. 1 (bottom). The bandwidth W and the density of states $N(E_F)$ to first order depend only on the inter-molecular π-electron overlap, illustrated in Fig. 2. With this picture in mind, and with the purpose to conduct a study of electron–phonon interactions, we consider a simple empirical tight-binding Hamiltonian [3, 31] of the form:

$$H_{TB} = \sum_{i\alpha} \epsilon_{i\alpha} C_{i\alpha}^{+} C_{i\alpha} + \sum_{i<j}^{nn} \sum_{\alpha\alpha'} t_{i\alpha j\alpha'} C_{i\alpha}^{+} C_{i\alpha'},$$

where the on-site energies $\epsilon_{i\alpha}$ and the nearest neighbor hopping integrals $t_{i\alpha, j\alpha'}$ are empirically determined parameters. We use a four state ($\alpha = s, p_x p_y p_x$) basis set. The Slater–Koster matrix elements (ϵ, t) are obtained from weighted fits to first-principles, LDA-type band structures of C_2, graphite and diamond at different interatomic separations. Two representative sets of parameters, as obtained by us [31] (TB1) and by Goodwin [32] (TB2) are listed in Table 1. The parameters are normalized to the intra-atomic distance d_0 in diamond. The scaling of these parameters with distance is an important and more subtle question. One can use the traditional d^{-2} dependence proposed for p-electron overlap [33]. Our fits to LDA results indicate a d^{-3} dependence of $t_{pp\pi}$ and a d^{-2} dependence of all other hopping integrals. Goodwin [32] proposes $d^{-2.8}$ for all hoppings. When calculating the electron–phonon coupling strength for intra-molecular vibrations we shall compare all different

Table 1. Tight binding parameters for carbon (in eV) for an inter-atomic separation of $d_0 = 1.55$ Å (diamond). TB1, TB2 refer to different models given in Refs 31 and 32, respectively

	TB1	TB2
ϵ_s	−7.3	−7.45
ϵ_p	0	0
$t_{ss\sigma}$	−3.63	−4.43
$t_{sp\sigma}$	+4.20	+3.79
$t_{pp\sigma}$	+5.38	+5.66
$t_{pp\pi}$	−2.24	−1.83

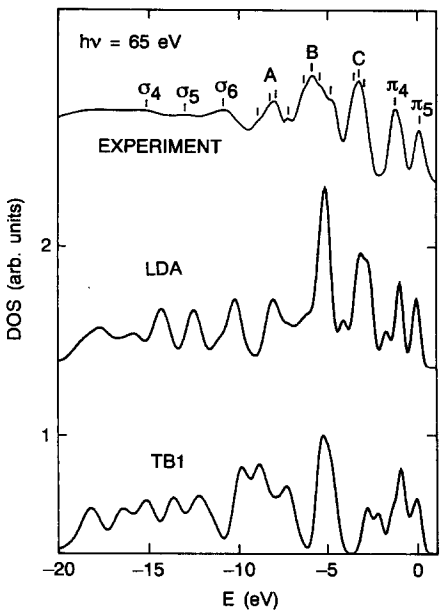

Fig. 3. Comparison of the valence electron density of states of C_{60} as measured by photoemission (top) (Ref. 15) and as calculated by the LDA pseudopotential scheme (middle) and the TB1 empirical tight binding scheme (bottom). The theoretical spectra are convoluted with an energy dependent Gaussian 'self-energy' function with width $0.23 + 0.02|\epsilon|$ (Ref. 19).

models. Inter-molecular distance dependence of t is empirically determined from the superconductivity results to be about $d^{-2.7}$ (see section 6). A comparison of the overall valence electron spectrum of C_{60} between LDA, TB1 and an experimental photoemission spectrum is shown in Fig. 3. The close similarity of the molecular features confirms the overall correctness of the theoretical models.

3. VIBRATIONAL STATES IN A_3C_{60}

As for the electronic states it is also instructive to subdivide the vibrations of A_3C_{60} into individual groups reflecting the molecular nature of the compound. In Fig. 4 a sketch of the full vibrational spectrum is shown. The highest frequency band (A) is due to intra-molecular vibrations of C_{60}. The highest modes are mostly tangential in character, while the modes at the lower end of the spectrum have mostly radial character. There are 174 modes grouped into one, three, four and five-fold degenerate representations. Experimentally, the modes have been studied by neutron scattering [34, 35], Raman scattering [36–39] and infrared absorption [37]. The Raman studies are of particular interest to us, since the symmetry selection rules of this process select the same identical modes that couple to the conduction electrons in the t_{1u} LUMO. These are two symmetric, one-fold degenerate A_{1g} modes and eight five-fold

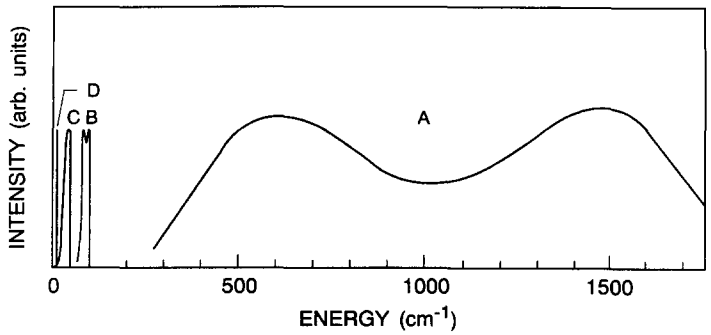

Fig. 4. Sketch of the complete vibrational spectrum of A_3C_{60}. Different groups of vibrations are emphasized. Intra-molecular vibrations are highest in energy (A), optic alkali vibrations are lower (B), followed by acoustic inter-molecular C_{60} vibrations (C) and C_{60} librations at very low energy (D).

degenerate H_g modes. The two A_g modes correspond to the (relatively low energy, $\sim 500\,cm^{-1}$) overall radial breathing mode and the (relatively high energy, $\sim 1500\,cm^{-1}$) tangential double-bond stretching mode. This latter mode can also be viewed as a tangential breathing of the 12 pentagons. The displacement patterns of the five-fold degenerate (*d*-like quadrupolar) H_g modes are more complex. They are depicted in Fig. 5, as calculated from a bond charge model. Detailed discussion of these modes can be found in several earlier studies [40–42]. In our work we have employed four different, approximate descriptions of these vibrations. These are a Keating-type model [43] with two parameters describing nearest neighbor bond–stretch (α) and bond–bend (β) forces. We used two different β/α ratios (0.1 and 0.3) with the overall scale adjusted to experiment. The value of 0.1 is close to what has been used previously to describe the vibrations of benzene [42] and the in-plane modes of graphite. However, Keating-type models, well suited for diamond-type sp^3 networks, work less well for planar sp^2 graphite. In fact, with only nearest neighbor interactions they do not stabilize any out-of-plane motion in planar graphite. In C_{60}, because of finite curvature, they are somewhat better suited. A further empirical model we use is the so-called bond–charge model, developed by Weber [44] for diamond and extended to graphite and C_{60} by Onida and Benedek [45]. In this model, Keating-like bond–stretch and bond–bend potentials are augmented by a (long-range) screened Coulomb interaction between adiabatic charges localized at the atoms and about midway between the atoms in the bonds. The strength of this interaction is one further empirical parameter. The fourth vibrational model we used is based on the MNDO empirical electronic structure method, with the results described in Ref. 40. In this well established method, vibrational eigenmodes are found from the second derivative of a parameterized electronic Hamiltonian. The parameters are fit to a large set of molecular energies and not specifically adjusted to C_{60}. In Table 2 we compare [46] the 10 Raman active mode frequencies ($2A_g + 8H_g$) of the four employed models with experimental results. The average deviations from experiment range from $\sim 3\%$ to $\sim 10\%$ with the empirical bond charge model giving the best overall agreement.

When C_{60} is condensed into a A_3C_{60} solid additional vibrational degrees of freedom appear of finite frequencies. Since the mass of alkali atoms is significantly smaller than that of C_{60} the vibrations of the ionic A_3C_{60} solid are well separated into three acoustic branches (C) of mostly C_{60} character at low frequencies ($\approx 50\,cm^{-1}$) and nine optic branches (B) of mostly alkali character at higher frequencies ($\approx 100\,cm^{-1}$). All frequencies are generally low because of the weak inter-molecular interactions, but they are increased in the intercalated material because of ionic Coulomb contributions. Experimentally, alkali induced, strongly dipole active modes are found near $80\,cm^{-1}$ using electron energy loss spectroscopy [47]. Finally, there is another class of very low frequency modes (D), corresponding to the librational motion of C_{60} molecules in their angular potential wells.

Table 2. Comparison of the measured eight H_g and two A_g Raman active modes of C_{60} to various theoretical models described in the text. The average deviation from experiment is given in the bottom row. All energies are in cm^{-1}

Mode	ω_p^{exp}	Keating $\beta/\alpha = 0.1$	Keating $\beta/\alpha = 0.3$	Bond charge	MNDO
$H_g(1)$	273	250	298	271	263
(2)	437	347	411	410	447
(3)	710	444	621	718	771
(4)	744	774	766	793	924
(5)	1099	1145	1162	1157	1261
(6)	1250	1299	1226	1218	1407
(7)	1428	1662	1500	1452	1596
(8)	1575	1718	1718	1691	1722
$A_g(1)$	497	492	476	499	610
(2)	1469	1678	1452	1455	1667
$\Delta\%$		11.9	5.8	3.2	10.7

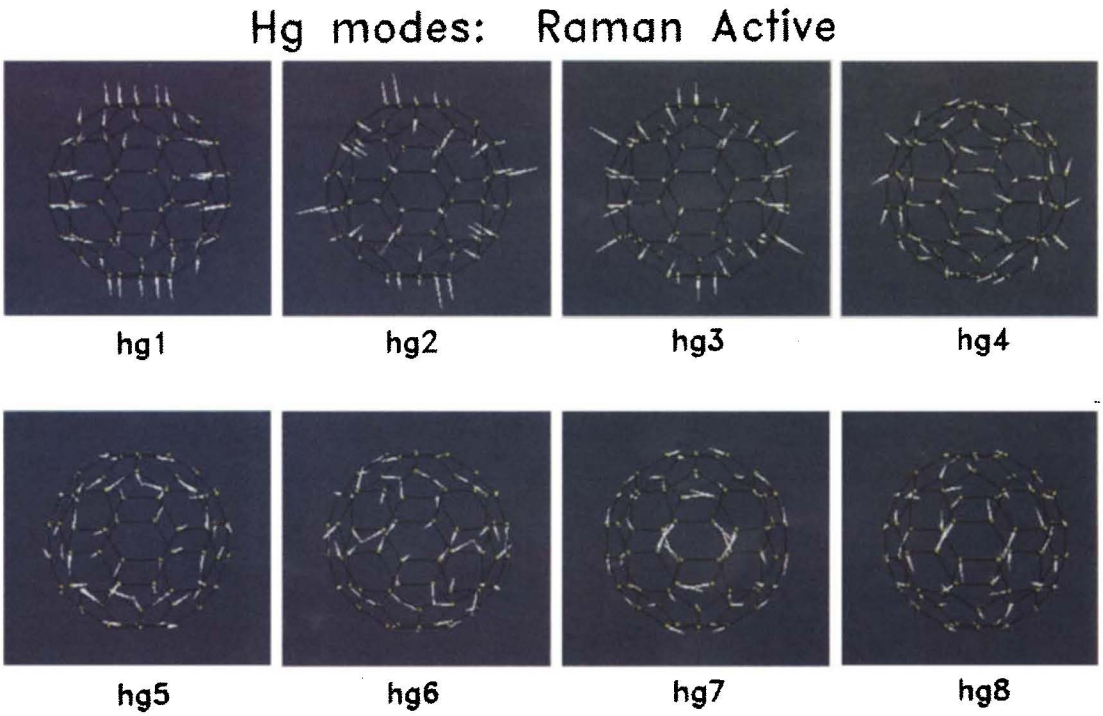

Fig. 5. Eigenvector representation of representative members of each of the eight (five-fold degenerate) H_g vibrational modes. These modes are both Raman active and couple to electrons in the t_{1u} LUMO (plot courtesy M. Grabow).

These modes have recently been identified in pure C_{60} by quasi-elastic neutron scattering [48] and by specific heat measurements [49]. They are in the 10–20 cm^{-1} regime and presumably at somewhat higher frequencies for the intercalated materials. In the context of our present investigations we make no particular effort to quantitatively describe vibrations other than the intra-molecular modes. As will become evident in the next section, for superconductivity coupling to electrons in the t_{1u} LUMO derived bands is dominated by these intra-molecular modes. Coupling to the low frequency modes may affect the normal state resistivity.

4. ELECTRON–PHONON COUPLING IN A_3C_{60}

In the BCS theory of superconductivity the dimensionless electron–phonon coupling constant is given by:

$$\lambda = \frac{2}{N(0)} \sum_{p,\mathbf{q}} \frac{1}{2K_p(\mathbf{q})} \sum_{\substack{n\mathbf{k} \\ n'\mathbf{k}'}} |I_{n\mathbf{k},n'\mathbf{k}'}(p,\mathbf{q})|^2 \, \delta(\epsilon_{n\mathbf{k}}) \, \delta(\epsilon_{n'\mathbf{k}'}), \quad (2)$$

where $\epsilon_{n\mathbf{k}}$ is the energy of the electronic Bloch state of band n with wavevector $\mathbf{k}$. The delta functions ensure the sum to be restricted to the Fermi surface. $K_p(\mathbf{q}) = M\omega_p^2(\mathbf{q})$ is the force constant of the pth photon with wavevector $\mathbf{q}$ and $I_{n\mathbf{k},n'\mathbf{k}'}(p,\mathbf{q})$ is the electron–phonon matrix element, linear in the phonon normal mode amplitudes. $N(0)$ is the density of states at the Fermi level per spin orientation. We now use a tight binding representation for the Bloch states [50]

$$\psi_{n\mathbf{k}}(\mathbf{r}) = \frac{1}{\sqrt{N}} \sum_{\substack{\tau\ell \\ \mathbf{R}}} c_{\tau\ell}(n\mathbf{k}) e^{i\mathbf{k}\mathbf{R}} \phi_\ell(\mathbf{r} - \mathbf{R} - \boldsymbol{\tau}) \quad (3)$$

with the sum running over all sites τ in the unit cell, all cells R and all orbitals ℓ, contributing to the t_{1u} manifold near E_F. Inserting (3) into (2), together with the phonon eigenmode representation in terms of individual atomic displacements $\mathbf{u}_\tau(p,\mathbf{q})$ we obtain:

$$\begin{aligned} I_{n\mathbf{k},n'\mathbf{k}'} = \sum_{\substack{\tau\ell \\ \tau'\ell'}} & C^*_{\tau\ell}(n\mathbf{k}) C_{\tau'\ell'}(n'\mathbf{k}') \\ & \times \sum_R \{\nabla_\tau \langle \phi_\ell(\mathbf{r} - \boldsymbol{\tau}) | H | \phi_{\ell'}(\mathbf{r} - \mathbf{R} - \boldsymbol{\tau}') \rangle\} \\ & \times \{\mathbf{u}_\tau(p,\mathbf{q}) e^{i\mathbf{k}'\mathbf{R}} \\ & - \mathbf{u}_{\tau'}(p,\mathbf{q}) e^{i\mathbf{k}\mathbf{R}}\} \, \delta(\mathbf{k} - \mathbf{k}' - \mathbf{q}). \end{aligned} \quad (4)$$

The crucial term in (4) is the first parenthesis, where the derivative of an atomic hopping matrix-element is calculated with respect to the motion of an atom at site τ. As pointed out early on, this gradient matrix element is proportional to the original matrix element itself. This observation is extremely useful in a molecular crystal with strongly different energy scales. It permits to neglect in (4) all contributions except those that modulate the strong *intra*-molecular π–π overlap of the t_{1u} states. In this limit of $t_{inter}/t_{intra} \to 0$, the sum in (4) can be further simplified [51] and one obtains:

$$\lambda = N(0)V = N(0) \sum_p V_p = N(0) \sum_{p,\mu} \frac{\mathrm{Trace}(I^2)_{p,\mu}}{9M\omega_p^2}, \quad (5)$$

where the trace corresponds to the (3×3) matrix in the t_{1u} subspace and summations of p and μ are over the normal modes p of an isolated C_{60} with their degeneracy index μ. These modes are normalized per C_{60} molecule. The quantity V_p in eqn (5) is just the average coupling energy in the (3×3) t_{1u} subspace.

The beauty of this result is that it directly relates to the adiabatic Jahn–Teller problem of an electron in the three-fold degenerate t_{1u} manifold coupled to distortions of the isolated C_{60} molecule. This relationship has recently been shown by Lannoo *et al.* [51] by revisiting the classic Jahn–Teller problem [52] of a three-fold degenerate electronic state coupled to five-fold degenerate distortions ($t_{1u} \times H_g$). Interestingly, the problem can be expressed as a special case of a tetrahedral defect of T_d symmetry coupled to modes of T and E symmetry (like the vacancy in silicon). The resulting static Jahn–Teller coupling energy is given in terms of the coupling matrix elements I as:

$$E_p(H_g) = \sum_\mu \frac{\mathrm{Trace}(I^2)_{p,\mu}}{15M\omega_p^2}. \quad (6)$$

Therefore the contribution V_p to λ in eqn (5) is

$$V_p = \tfrac{5}{3} E_p(H_g). \quad (7)$$

for H_g modes. Analogously one finds for the totally symmetric A_g modes

$$V_p = \tfrac{2}{3} E_p(A_g). \quad (8)$$

Using the different electronic structure models and the different phonon models we can now numerically evaluate $V = \Sigma_p V_p$. The results are compiled in Tables 3–5. Looking first at Table 5 we see that, for a given electronic structure model (e.g. column 3, TB1 with $n_{pp\pi} = 3$), the values for V are reasonably constant, except for the MNDO model. For a given phonon model (e.g. row 3, the bond charge model) the strength of the coupling depends of course strongly ($\sim n^2$) on the distance exponent n. Comparing with the LDA results an exponent near $n \approx 2.5$ seems to be appropriate for the present situation. Inspecting the results in more detail (Tables 3, 4) one

Table 3. Electron–phonon coupling constants $V = \Sigma_p V_p$ (in meV) for individual modes p and the logarithmically averaged frequency ω_{log} (in cm^{-1}) used for estimates of T_c (see eqn (10)). Here the results are for different phonon models and the same TB1 electronic tight-binding model with a $n_{pp\pi} = 3$ distance dependence of the matrix elements

Mode	Keating $\beta/\alpha = 0.1$	Keating $\beta/\alpha = 0.3$	Bond charge	MNDO
$H_g(1)$	1.1	11.0	9.4	1.4
(2)	3.2	5.1	3.2	1.8
(3)	26.6	16.0	7.6	6.3
(4)	3.7	11.6	10.8	0.7
(5)	0.1	0.2	0.2	0.8
(6)	0.0	0.0	1.1	1.1
(7)	2.2	11.2	18.5	18.3
(8)	35.9	27.1	22.2	16.3
V	72.8	82.2	73.0	46.7
ω_{log}	786	887	982	1320

can see that the spectral distribution of V_p is rather similar in all cases, except for the phonon calculations with the Keating ($\beta/\alpha = 0.1$) model and the MNDO model. In all other models roughly one-half of the oscillator strength comes from the lowest four (radial) modes and one half from the highest four (tangential) modes. These general results are in contrast with the MNDO results of Ref. 2 which report about 80% of the contributions to V to originate from the highest two modes ($H_g(7)$, $H_g(8)$). We shall, in the next section discuss experiments that do measure quantities related to these coupling strengths.

In the limit $t_{inter}/t_{intra} \to 0$, which we discussed so far, no $q = k - k'$ dependence of the scattering exists. For the Jahn–Teller types symmetry lowering H_g modes, the scattering is thus inter-band (off-diagonal in the t_{1u} LUMO manifold) on an individual C_{60} molecule. The coupling to the A_g symmetric modes merits further discussion. The mode coupling is diagonal in the t_{1u} space and therefore does not scatter on an individual molecule. The $q = 0$ limit

Table 4. Electron–phonon coupling constants $V = \Sigma_p V_p$ (in meV) for individual modes p and the logarithmically averaged frequency ω_{log} (in cm^{-1} used for estimates of T_c (see eqn (10)). Here the results are for different electronic models and the same bond-charge phonon model. The LDA results are obtained by the 'frozen phonon' method (Ref. 3)

Mode	TB1 $n = 2$	TB1 $n_{pp\pi} = 3$	TB2 $n = 2.8$	LDA
$H_g(1)$	3.0	9.4	4.7	8.0
(2)	2.4	3.2	2.9	7.0
(3)	6.0	7.6	8.5	4.0
(4)	4.8	10.8	7.7	7.0
(5)	0.0	0.2	0.1	1.0
(6)	0.6	1.1	0.6	3.0
(7)	7.0	18.5	11.1	13.0
(8)	8.4	22.2	13.4	9.0
V	32.2	73.0	49.1	52.0
ω_{log}	939	982	946	950

Table 5. Summary of calculated electron–phonon matrix elements V (in meV). The columns correspond to electronic structure models, the rows to phonon models. Details are in the text. The result labelled (*) is extracted from Ref. 2

	LDA	TB1 $n = 2$	TB1 $n_{pp\pi} = 3$	TB2 $n = 2.8$	MNDO
Keating $\beta/\alpha = 0.1$		38.1	72.8	57.4	
Keating $\beta/\alpha = 0.3$		37.6	82.2	58.0	
Bond charge	52.0	32.2	73.0	49.1	
MNDO		21.6	46.7	32.8	56.0*

corresponds simply to an overall shift, as also pointed out in Ref. 2. The modes can, however, scatter between molecules for a finite t_{inter} and a finite q. In this case the scattering strength would again be given by the strong t_{intra}. For finite doping, such as in A_3C_{60}, however, the inter-molecular potential produced by a $q \neq 0$ A_g mode is likely to be screened out, effectively eliminating the contributions of A_g modes to the electron–phonon coupling parameter in the metallic compound. Screening also eliminates the coupling to the alkali modes. Since the LUMO wavefunctions have vanishingly small amplitudes at the alkali sites, only long-range potentials could scatter [4]. These are, however, efficiently screened in the metallic compounds. This is in contrast to on-ball Jahn–Teller modes which directly modulate nearest neighbor wavefunction overlap. Here screening has only a quantitative effect.

Equation (5) shows that the dimensionless coupling constant is proportional to the density of states $N(0)$ of electrons at E_F. Although this quantity should in principle be available from calculations and/or experiments, in practice the situation is still unclear. On the theoretical side the problems are mainly due to uncertainties and disorder in the orientational arrangement of C_{60} molecules. Intra-molecular bonding merely determines that $N(0)$ derives from a well-isolated three-fold degenerate t_{1u} LUMO. Although this is rather important, the weak inter-molecular interactions determine the value of $N(0)$. On an approximate scale, $N(0) = 3/W$ per spin, where W is the t_{1u} conduction band width. Most calculations [3, 19, 20], in reasonable agreement with each other show $W \approx 0.5$ eV resulting in an average $N(0) \approx 6$ states/eV–spin–C_{60}. However, the inter-molecular density of states has considerable structure [5], some of which may be washed out by disorder which can drastically change this value. A recent model calculation [53] supports this view. On the experimental side, large variations exist in reported estimates for $N(0)$. Photoemission data [54] are interpreted to give small values, $N(0) \approx 1$–2. Difficulties here are

associated with hole lifetime effects and/or surface sensitivity. Susceptibility measurements [55] suggest values in the range of $N(0) \approx 10$–15, while NMR data [56] suggest even larger values $N(0) \gtrsim 20$. The difficulties here are associated with extracting 'bare' density of states values in the presence of interactions and disorder. The questions are largely unsettled at this time and we have to consider reasonable ranges of $N(0)$.

5. SUPERCONDUCTIVITY

The complete theory of superconductivity, given by Eliashberg allows one to calculate T_c, given the interaction strengths and their respective frequency distributions. For the attractive electron–phonon interaction, these are the coupling parameters $\lambda_p = N(0) \cdot V_p$ and the vibrational frequencies ω_p. Less detail is known for the repulsive Coulomb interaction μ, which we shall discuss below. An approximate, explicit formula for T_c has been given by McMillan [57], which works remarkably well for not too strong coupling. For the present case, we have tested the validity of McMillan's formula by solving Eliashberg's equation numerically [58] for a variety of scenarios. We have found that for the vibrational intra-molecular coupling of C_{60}, McMillan's formula gives excellent results. Then T_c is given by

$$T_c = \frac{\hbar\omega_{\log}}{1.2K_B} \exp\left[\frac{-1.04(1+\lambda)}{\lambda - \mu^* - 0.62\lambda\mu^*}\right], \tag{9}$$

where the logarithmically averaged phonon frequency $\omega_{\log}$ is given by

$$\ln \omega_{\log} = \frac{1}{\lambda} \sum_p \lambda_p \ln \omega_p, \tag{10}$$

with $\lambda = \Sigma_p \lambda_p$. Values for $\omega_{\log}$ have been calculated for the various models and some are indicated in Tables 3 and 4. They are remarkably constant and typically of order 800–1000 cm^{-1} or 1150–1450 K (with the exception of the MNDO results of Ref. 2).

The effective Coulomb interaction μ^* is reduced from the full Coulomb repulsion μ by retardation via the approximate relationship [59]

$$\left(\frac{1}{\mu^*}\right) = \left(\frac{1}{\mu}\right) + \ln\left(\frac{\omega_{el}}{\omega_{ph}}\right). \tag{11}$$

Here ω_{el} is the characteristic cut-off frequency for Coulomb interactions while $\omega_{ph} \approx \omega_{\log}$. The effectiveness of retardation has been questioned [60] for C_{60} molecular solids on grounds that the bandwidth W for inter-molecular hopping is comparable to $\hbar\omega_{\log}$. It is, however, important to realize that the electronic structure of A_3C_{60} is strongly molecular only for the valence states and the first few conduction bands. Higher lying states intermix with the alkali states and are truly extended throughout the solid. Coulomb scattering into these higher lying states allows electrons therefore to hop off the C_{60} molecules at a much faster rate than that given by W. The correct frequency to use in eqn (11) is therefore a characteristic A_3C_{60} plasma frequency of order 10 eV or higher. Recent calculations [61] and electron energy loss experiments [62] show strong structures in the scattering form factor $S(q, \omega)$ near 6 eV and 25 eV, due to C_{60}, π and σ plasmons, respectively. We therefore believe that the Coulomb repulsion in A_3C_{60} is rather standard, i.e. a value of $U \approx$ few eV for carbon orbitals yields a $\mu = N(0) \cdot U$ of order 0.5–1.0 for the molecule which is then renormalized via retardation to values of $\mu^* \approx 0.1$–0.2. Isotope measurements, discussed below are consistent with these values.

It is clear that with all the uncertainties in $N(0)$, V and μ^*, T_c cannot be reliably calculated. Inversely, however, the observed T_c values can well be explained with parameters within the discussed range. For instance, for a $\hbar\omega_{\log} \approx 1400$ K as obtained from the bond charge model, a $V \approx 50$ meV which is about the calculated LDA value (see Table 5), an average $N(0) \approx 14$ and a $\mu^* \approx 0.2$ one obtains $T_c \approx 20$ K which is the observed T_c for K_3C_{60}. The important question is whether these estimates sensibly explain observed trends and whether the overall picture is consistent with all experiments.

It was noted earlier [63] that T_c scales monotonically with the A_3C_{60} lattice constants upon chemical alkali substitution. This observation is beautifully confirmed by the present scenario. The molecular nature of A_3C_{60} 'factors' all quantities in real space. The electron–phonon coupling matrix element V, and the prefactor $\hbar\omega_{\log}$ are intra-molecular quantities of C_{60} and should be invariant. If we also assume μ^* to be constant to first order, only the density of states $N(0)$ varies from compound to compound. To first-order, it scales with inter-molecular distance d as

$$N(0) \sim \frac{1}{W} \sim \frac{1}{t^0_{\text{inter}}}\left(\frac{d}{d_0}\right)^n. \tag{12}$$

In Fig. 6 and Table 6 we show how this simple argument used with the selected values given above and a distance scaling of $n = 2.7$ beautifully explains all observed trends. This value of n empirically adjusted is within the range expected for inter-molecular interactions [20].

The effect of chemical pressure is fully equivalent to mechanical pressure. Also shown in Fig. 6 and Table 6 are experimental results [64–66] obtained by applying hydrostatic pressure to K_3C_{60} (○) and to

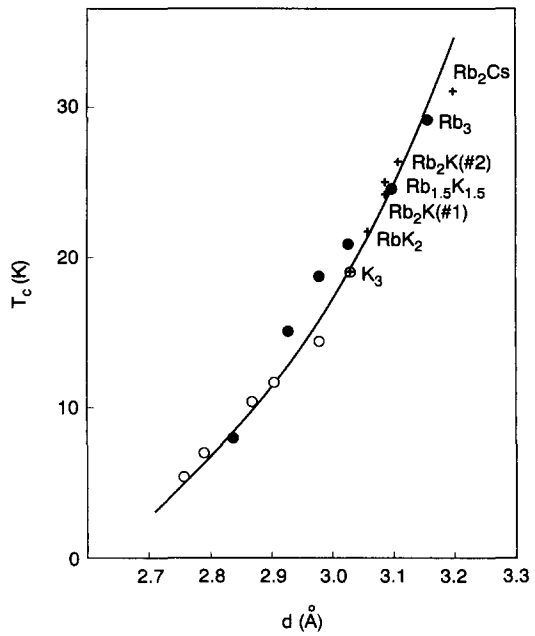

Fig. 6. Experimentally observed variation in T_c with lattice constant variations, converted here into an approximate surface distance between C_{60} molecules. Shown are the data for chemically substituted compounds (+), Ref. 63, and those obtained from K_3C_{60} (○) and Rb_3C_{60} (●) via mechanical pressure (Ref. 66). The solid line is the calculated variation of T_c using McMillan's formula and the parameters discussed in the text.

Rb_3C_{60} (●). The results follow the same curve. This shows unambiguously that there is no alkali isotope effect. Rb_3C_{60} reduced to the volume of K_3C_{60} has virtually the same T_c as K_3C_{60}. This contradicts the model for superconductivity proposed in Ref. 4.

The situation is drastically different for carbon isotope substitution. According to our model for superconductivity we expect $\hbar\omega_{\log}$ to change $\sim 1/\sqrt{M}$. Since $\hbar\omega_{\log}$ enters T_c as prefactor and in the reduction of μ^*, we expect from McMillan's formula

$$T_c \sim M^{-\alpha} \tag{13}$$

with

$$\alpha = \frac{1}{2}\left\{1 - \left(\mu^* \ln \frac{\hbar\omega_{\log}}{1.2kT_c}\right)^2 \frac{1+0.62\lambda}{1+\lambda}\right\}.$$

In Table 7 we illustrate the variation of α for two scenarios. One corresponding to our model with $\hbar\omega_{\log} \approx 1400$ K and one for a hypothetical low energy phonon model with $\hbar\omega_{\log} \approx 200$ K. In both cases λ and μ^* have been chosen to reproduce the $T_c \approx 29$ K for Rb_3C_{60}. For the model developed here and with $\mu^* = 0.2$ we expect a reduction of α from 0.5 to 0.29. This is in excellent agreement with recent measurements by Ramirez *et al.* [68] which indicate $\alpha = 0.37 \pm 0.05$ and by Chen and Lieber [69] who find $\alpha = 0.30 \pm 0.06$ for K_3C_{60}. Very different results ($\alpha > 1$) have been reported by Ebbesen *et al.* [70], but for rather incomplete isotope substitution.

The strong coupling scenario does not yield any appreciable reduction of α, unless one goes beyond the range of validity of McMillan's theory [67]. While this agreement seems to confirm our model we have to caution that sizeable isotope effects can in principle also occur for different reasons. Inspection of Fig. 6 shows that the observed ≈ 0.5 K change of T_c upon C^{13}/C^{12} substitution could also be accounted for if the lattice parameter was reduced by ≈ 0.01 Å.

Table 6. Compilations of experimental T_c values vs lattice constants a. The chemical substitution data are from Ref. 63, the Rb_3 and K_3 pressure data are from Ref. 66. The inter-molecular distance d is approximated using a C_{60} radius of 3.52 Å. The calculated values are obtained from scaling the K_3C_{60} λ-value using a $n = 2.7$ distance variation of $N(0)$ (see eqn (12) in text). T_c is calculated with $\mu^* = 0.2$. The table is illustrated in Fig. 6

	a	d	T_c^{exp}	T_c^{calc}	λ^{calc}
Rb_2Cs	14.49	3.20	31.3	34.9	0.85
Rb_3	14.44	3.16	29.4	31.0	0.82
Rb_2K	14.36	3.11	26.4	25.9	0.78
$Rb_{1.5}K_{1.5}$	14.34	3.09	25.2	24.7	0.77
RbK_2	14.30	3.06	21.8	22.3	0.75
K_3	14.25	3.03	19.3	19.9	0.73
Rb_3	14.44	3.16	29.4	34.9	0.85
	14.35	3.10	24.8		
	14.27	3.03	21.0		
	14.18	2.98	18.9		
	14.11	2.93	15.2		
	13.98	2.84	8.1	8.0	0.61
K_3	14.25	3.03	19.3	19.9	0.73
	14.18	2.98	14.5		
	14.09	2.91	11.9		
	14.03	2.87	10.6		
	13.92	2.79	7.1		
	13.87	2.76	5.5	5.1	0.57

Table 7. Calculated isotope shift exponents for a weak coupling model (top) and a strong coupling model (bottom). The values of λ, μ^* are chosen to reproduce the T value of 29 K (Rb_3C_{60}) using McMillan's formula [57]. The model developed in this paper corresponds to $\lambda = 0.81$ which together with $\mu^* = 0.2$ predicts $\alpha = 0.29$. The measured value is 0.32 ± 0.05 (Ref. 68)

$\hbar\omega_{\log} = 1400$ K		
λ	μ^*	α
0.39	0.0	0.50
0.58	0.1	0.45
0.81	0.2	0.29
1.09	0.3	0.04
$\hbar\omega_{\log} = 200$ K		
λ	μ^*	α
1.5	0.0	0.5
2.1	0.1	0.49
2.9	0.2	0.46
4.2	0.3	0.41

Anharmonic zero-point motion effects [71] could in principle account for this. Precision lattice parameter measurements are needed to clear up this ambiguity. For models where superconductivity derives from intra-molecular correlations [5, 6] isotope effects can also be obtained by similar arguments from on-ball zero point fluctuations.

The coupling of the Jahn–Teller type modes to conduction electrons modifies these modes themselves. As proposed by Allen [72], these mode self-energy effects should be observable. The self-energy can be expressed in a phonon linewidth (Lorentzian full width)

$$\gamma_p = \pi\omega_p^2 N(0)^2 \frac{V_p}{d_p} \tag{14}$$

and a frequency shift

$$|\Delta\omega_p| = \omega_p N(0) \frac{V_p}{d_p},$$

where the coupling strength V_p is given in eqn (5) and where d_p is the degeneracy of mode p. In Table 8 we list these phonon self-energy parameters for the case of the bond charge phonon model and the LDA frozen phonon couplings (see Table 4). A value of $N = 14$ states/eV–spin–C_{60} was used, as appropriate for K_3C_{60}. We see significant phonon linewidth broadening. Particularly affected are the higher frequency modes due to the ω_p^2 factor in eqn (14). These results can be compared to Raman [36, 38, 39] and neutron [35] scattering data, contrasting the insulating C_{60} and A_6C_{60} phases with the metallic A_3C_{60} phase.

In the case of Raman scattering the (dispersionless) intra-molecular modes are probed near $q \approx 0$. In a perfect crystal the continuum of t_{1u}-derived electronic states near E_F couples to these modes for $E(k) = \omega_{ph}$ near k_F, which is much larger. There is, however, as stated earlier, considerable disorder (in particular orientational) in these materials which does not only give a short mean free path but which also should destroy q-conservation and allow for Raman scattering to probe the electron–phonon coupling. This was studied experimentally by several groups [36, 38, 39] who have identified substantial coupling of the H_g modes in metallic A_3C_{60} to a continuum which is absent in the insulating phases (C_{60}, A_6C_{60}). Coupling is observed in all cases to both low energy (radial) and high energy (tangential) modes, in general agreement with the present calculations. The coupling to the low energy H_g modes, in particular $H_g(2)$ is also clearly observed by neutron scattering [35]. Line frequency shifts are a more subtle problem, since other effects occur in going from C_{60} to A_3C_{60}, e.g. crystal field shifts due to the A^+ ions, weakening of the C_{60} bonds due to occupying the antibonding t_{1u} level, etc. Detailed comparisons between theory and experiment should, however, become possible.

Table 8. Phonon self-energies calculated (eqn (14)) from the parameters of the LDA/bondcharge model. A value of $N = 14$ states/eV–spin–C_{60} and the values of V_p in Table 4 were used. All energies are given in cm^{-1}. The line width γ is a Lorentzian full width at half maximum

	ω_p^{calc}	ω_p^{exp}	γ_p	$\lvert\Delta\omega_p\rvert$
$H_g(1)$	271	273	7	6
(2)	410	437	15	8
(3)	718	710	23	7
(4)	793	744	56	15
(5)	1157	1099	15	3
(6)	1218	1250	50	9
(7)	1452	1428	307	45
(8)	1691	1575	192	24

We summarize the scenario developed here for superconductivity in A_3C_{60}. The parameters are as follows: relatively high energy phonons with $\hbar\omega_{log} \approx 1400$ K couple with weak to intermediate strength of $\lambda \approx 0.73$, subject to a reasonably large Coulomb repulsion of $\mu^* \approx 0.2$ to yield T_c near 20 K for K_3C_{60}. We are thus not in the strong coupling limit and expect the BCS value of $2\Delta \approx 3.5kT_c$ for the superconducting gap and a coherence length of $\xi_0 \approx 130$ Å. NMR [73] and optical [74] data seem to indicate a BCS gap value, while point contact tunneling [75] yields larger values. Coherence lengths of ≈ 150 Å have been inferred from H_{c2} measurements [76] on granular films; much smaller values are typically quoted [75] using a clean limit interpretation.

Can we use what we learned here and extrapolate to new, hypothetical materials? The obvious first choice is C_{60} itself with different doping levels. If one could hole-dope C_{60} the conduction electrons would be situated in a band derived from a five-fold degenerate h_u level. Calculations [20] show the width of this band also to be about 0.5 eV, so $N(0)$ could be larger by a factor ~ 1.7 over the electron doped case. The coupling V can be calculated analogously to the electron case and is found to be smaller by a factor of ~ 1.4, such that the overall coupling strength λ becomes only somewhat larger. Although different modes couple, $\hbar\omega_{log}$ is about the same, so we expect a T_c in the same range as for the electron doped case. Similar studies for the next higher conduction band complexes (three-fold t_{1g} and three-fold t_{2u}) yield coupling strengths V, increased by $\sim 10\%$ and $\sim 40\%$ over the t_{1u} LUMO value, respectively. These findings may be of relevance for the recently discovered Ca intercalated materials [78].

Coupling V derives some of its contributions from coupling to lower energy radial or transverse modes. These modes couple to π-like electrons only for

curved geometries. In fact, in graphite there is no first order coupling to transverse modes for symmetry reasons, which we suggested [3] to be the reason why T_c is much lower in intercalculated graphite. (The density of states there is comparable [79] to A_3C_{60}.) Reversing the argument we may increase T_c if we find a highly symmetric molecule (with high electronic degeneracies) exhibiting a larger curvature than C_{60}. We have studied the hypothetical C_{20} molecule (only pentagons) which is insulating in its 2+ charge state. The symmetry of the LUMO is four-fold degenerate G_u which couples to A_g, G_g and H_g modes. The coupling V is found to be indeed about 1.5 times stronger than in C_{60}. Chemically, however, the atoms have near perfect sp^3 bond angles and the dangling bonds make C_{20} probably highly reactive.

6. CONCLUSIONS

We have examined the electronic and vibrational structure of A_3C_{60} compounds in detail and found by direct calculations that the Jahn–Teller type intramolecular modes do efficiently couple to the conduction electrons induced by alkali intercalation. Since the frequencies of these modes are high, they should be efficient for superconductivity. The coupling (V) is largely an isolated molecule property and can be derived from Jahn–Teller type studies. The hopping between the molecules is the second important ingredient in that it determines the kinetic energy or the density of states (N) of conduction electrons. Details are probably washed out by orientational disorder. The dimensionless BCS coupling parameter $\lambda = NV$ is then factorized in real space, a picture which is beautifully confirmed by several experiments, such as studies of chemical or mechanical pressure affecting T_c and vibrational linewidth studies in Raman or neutron experiments. Moreover, the absence of any alkali isotope effect and the observation of a strong effect upon carbon isotope can be quantitatively explained.

In spite of all these obvious confirmations the scenario developed here puts A_3C_{60} close to edge of validity of the underlying BCS model. The electron kinetic energy is only a few times larger than the average phonon energy $\hbar\omega_{\log}$ and Migdal's approximation used in BCS theory becomes less appropriate [80]. However, the factorization in real space may be helpful here too. Furthermore, estimates show that the kinetic energy is probably not much larger than the intra-molecular Coulomb repulsion [21, 81]. Further reduction of the kinetic energy, by e.g. increasing the lattice constant should ultimately lead to magnetic instabilities [82] limiting a further increase in T_c.

Acknowledgements—We thank W. Zhong and Y. Wang for assistance with numerical calculations and many of our colleagues for discussions of their results.

REFERENCES

1. Hebard A. F., Rosseinsky M. J., Haddon R. C., Murphy D. W., Glarum S. H., Palstra T. T. M., Ramirez A. P. and Kortan A. R., *Nature* **350,** 600 (1991).
2. Varma C. M., Zaanen J. and Raghavachari K., *Science* **254,** 989 (1991).
3. Schlüter M. A., Lannoo M., Needels M., Baraff G. A. and Tomanek D., *Phys. Rev. Lett.* **68,** 526 (1992).
4. Zhang F. C., Ogato M. and Rice T. M., *Phys. Rev. Lett.* **67,** 3452 (1991).
5. Charkavarty S., Gelfand M. P. and Kivelson S., *Science* **254,** 970 (1991).
6. Baskaran G. and Tossati E., *Current Science* **61,** 33 (1991).
7. Johnson K. H., McHenry M. E. and Cloughtery D. P., *Physica C* (1992) submitted.
8. Mazin I. I., Rashkeev S. N., Antropov V. P., Jepsen O., Liechtenstein A. I. and Andersen O. K., *Phys. Rev.* (1992) submitted.
9. Stollhoff G., *Phys. Rev.* **B44,** 10,998–11,000 (1991).
10. Pietronero L., preprint.
11. Martins J. L. and Troullier N., preprint.
12. Yannoni C. S., Bernier R. P., Bethune D. S., Meijer G. and Salem J. R., *J. Am. Chem. Soc.* **113,** 3190 (1991).
13. Fleming R. M., Siegrist T., Marsh P. M., Hessen B., Kortan A. R., Murphy D. W., Haddon R. C., Tycko R., Dabbagh G., Mujsce A. M., Kaplan M. L. and Zahurak S. M., *Mater. Res. Soc. Symp. Proc.* **206,** 691 (1991).
14. Hadon R. C., Brus L. E. and Raghavachari K., *Chem. Phys. Lett.* **125,** 459 (1986).
15. Weaver J. H., Martins J. L., Komeda T., Chen Y., Ohno T. R., Kroll G. H., Troullier T., Hauffer R. E. and Smalley R. E., *Phys. Rev. Lett.* **66,** 1741 (1991).
16. Zhang Q., Yi J. Y. and Berhnolc J., *Phys. Rev. Lett.* **66,** 2633 (1991).
17. Saito S. and Oshiyama A., *Phys. Rev. Lett.* **66,** 2637 (1991).
18. Feuston B. P., Andreoni W., Parrinello M. and Clementi E., *Phys. Rev.* **B44,** 4056 (1991).
19. Troullier N. and Martins J. L., to be published.
20. Satpathy S., Antropov V. P., Andersen O. K., Jepsen O., Gunnarsson O. and Liechtenstein A. I., *Phys. Rev.* submitted (1992).
21. Gunnarsson O., Satpathy S., Jepsen O. and Andersen O. K., *Phys. Rev. Lett.* **67,** 3002 (1991).
22. Yannoni C. S., Johnson R. D., Meijer G., Bethune D. S. and Salem J. R., *J. Phys. Chem.* **95,** 9 (1991).
23. Tycko R., Haddon R. C., Dabbagh G., Glarum S. H., Douglass D. C. and Mujsce A. M., *J. Phys. Chem.* **95,** 518 (1991).
24. Heiney P. A., Fischer J. E., McGhie A. R., Romanow W. J., Denenstein A. M., McCauley J. P., Smith A. B. and Cox D. E., *Phys. Rev. Lett.* **66,** 2911 (1991).
25. Tycko R., Dabbagh G., Fleming R. M., Haddon R. C., Makhija A. V. and Zahurak S. M., *Phys. Rev. Lett.* **67,** 1886 (1991).
26. Hu R., Egami T., Li F. and Lannin J. S., preprint.
27. Stephens P. W., Mihaly L., Lee P. L., Whetten R. L., Huang S.-M., Kaner R., Diedrich F. and Holezer K., *Nature* **351,** 632 (1991).
28. Murphy D. W., Rosseinsky M. J., Fleming R. M., Tycko R., Ramirez A. P., Haddon R. C., Siegrist T., Dabbagh G., Tully J. C. and Walstedt R. E., *J. Phys. Chem. Solids* **53,** 1321 (1992).

29. Erwin S. C. and Pickett W. E., *Science* **254,** 842 (1991).
30. Martins J. L. and Troullier N., *Phys. Rev.* (1992) submitted.
31. Tomanek D. and Schlüter M., *Phys. Rev. Lett.* **67,** 2331 (1991).
32. Goodwin L., *J. Phys. C* **3,** 3869 (1991).
33. Harrison W. A., *Phys. Rev. B* **27,** 3592 (1991).
34. Cappelletti R. L., Copley J. R. D., Kamitakahara W. A., Li F., Lannin J. S. and Ramage D., *Phys. Rev. Lett.* **66,** 3261 (1991).
35. Prassides K., Tomkinson J., Christides C., Rosseinsky M. J., Murphy D. W. and Haddon R. C., *Nature* **354,** 462 (1991).
36. Duclos S. J., Haddon R. C., Glarum S. H., Hebard A. F. and Lyons K. B., *Science* **254,** 1625 (1991).
37. Bethune D. S., Meijer G., Tang W. C., Rosen H. J., Golden W. G., Seki H., Brown C. A. and de Vries M. S., *Chem. Phys. Lett.* **179,** 181 (1991).
38. Mitch M. G., Chase S. J. and Lannin J. S., *Phys. Rev. Lett.* **68,** 883 (1992).
39. Zhou P., Wang K., Rao A. M., Eklund P. C., Dresselhaus G. and Dresselhaus M. S., *Phys. Rev.* submitted (1992).
40. Stanton R. E. and Newton M. P., *J. Phys. Chem.* **92,** 2141 (1988).
41. Brendsdal E., *Spec. Lett.* **24,** 319 (1988).
42. Weeks D. E. and Harter W. G., *J. Chem. Phys.* **90,** 4744 (1989).
43. Martin R., *Phys. Rev. B* **4,** 4005 (1970).
44. Weber W., *Phys. Rev. B.* **15,** 4789 (1977).
45. Onida G. and Benedek G., *Europhys. Lett.* submitted (1992).
46. We thank K. Raghavachati for providing us with the MNDO C_{60} vibrational eigenvectors and G. Onida for his bond charge model results.
47. Rowe J., Malic R. A., Chaban E. E. and Haddon R. C., to be published.
48. Neuman D. A., Copley J. R. D., Kamitakahara W. A., Rush J. J., Cappelletti R. L., Coustel N., McCauley J. P., Fisher J. E., Smith III A. B., Creegan K. M. and Cox D. M., preprint.
49. Beyermann W. P., Hundley M. F., Thompson J. D., Diederich F. N. and Grüner G., preprint.
50. Varma C. M., Blount E. I., Vashista P. and Weber W., *Phys. Rev. B* **19,** 6130 (1979).
51. Lannoo M., Baraff G. A., Schlüter M. and Tomanek D., *Phys. Rev. B* **44,** 1210 (1991).
52. O'Brien M. C., *J. Phys. C* **4,** 2524 (1971).
53. Gelfand M. P. and Lu J. P., *Phys. Rev. Lett.* **68,** 1050 (1992).
54. Chen C. T., Tjeng L. H., Rudolf P., Meigs G., Rowe J. E., Chen J., McCauley J. P., Smith A. B., McGhie A. R., Romanow W. J. and Plummer E., *Nature* **352,** 603 (1991).
55. Ramirez A. P., Rosseinsky M. J., Murphy D. W. and Haddon R. C., to be published.
56. Tycko R., Dabbagh G., Rosseinsky M. J., Murphy D. W., Fleming R. M., Ramirez A. P. and Tully J. C., *Science* **253,** 884 (1991).
57. McMillan W. L., *Phys. Rev.* **167,** 331 (1968).
58. Eliashberg G. M., *JETP* **11,** 696 (1960). We thank P. B. Allen for providing us with his Eliashberg code.
59. Morel P. and Anderson P. W., *Phys. Rev.* **125,** 1263 (1962).
60. Anderson P. W., preprint (1991).
61. Bertsch G. F., Bulgac A., Tomanek D. and Wang Y., preprint (1991).
62. Gensterblum G., Pineaux J. J., Thiry P., Candano R., Vigneron J. P., Lambin P. and Lucas A. A., *Phys. Rev. Lett.* **67,** 2171 (1991).
63. Fleming R. M., Ramirez A. P., Rosseinsky M. J., Murphy D. W., Haddon R. C., Zahurak S. M. and Makhija A. V., *Nature* **352,** 787 (1991).
64. Schirber J. E., Overmyer D. L., Wang H. H., Williams J. M., Carlson D. D., Kini A. M., Pellin M. J., Welp U. and Kwok W.-K., *Physica C* **178,** 137 (1991).
65. Sparn G., Thompson J. D., Huang S.-M., Kaner R. B., Diederich F., Whetten R. L., Gruner G. and Holczer K., *Science* **252,** 1829 (1991).
66. Zhou O., Vaughn G. B. M., Zhu Q., Fischer J. E., Heiney P. A., Coustel N., McCauley J. P. and Smith A. B., preprint.
67. Kresin V. Z., *Phys. Lett.* **A122,** 434 (1987).
68. Ramirez A. P., Kortan A. R., Rosseinsky M. J., Duclos S. J., Mujsce A. M., Haddon R. C., Murphy D. W., Makhija A. V., Zahurak S. M. and Lyons K. B., *Phys. Rev. Lett.* **68,** 1058 (1992).
69. Chen C. C. and Lieber C. M., preprint.
70. Ebbesen T. W., Tsai J. S., Tanigaki K., Tabuchi J., Shimakawa Y., Kubo Y., Hirosawa I. and Mizuki J., *Nature* **355,** 620 (1992).
71. Fisher D. S., Millis A. J., Shraiman B. and Bhatt R. N., *Phys. Rev. Lett.* **61,** 482 (1988).
72. Allen P. B., *Phys. Rev. B* **6,** 2577 (1972).
73. Tycko R., Dabbagh G., Rosseinsky M. J., Murphy D. W., Ramirez A. P. and Fleming R. M., preprint.
74. Rotter L. D., Schlesinger Z., McCauley J. P., Jr., Coustel N., Fischer J. E. and Smith A. B., III, preprint.
75. Zhang Z., Chen C.-C., Kelty S. P., Dai H. and Lieber C. M., *Nature* **253,** 333 (1991).
76. Palstra T. T. M., Haddon R. C., Hebard A. F. and Zaanen, *J. Phys. Rev. Lett.* **68,** 1054 (1992).
77. Sparn G., Thompson J. D., Whetten R. L., Huang S. M., Kaner R. B., Diederich F., Grüner G. and Holczer K., *Phys. Rev. Lett.* **68,** 1228 (1992).
78. Kortan A. R., Kopylov N., Glarum S. H., Gyorgy E. M., Ramirez A. P., Fleming R. M., Thiel F. A. and Haddon R. C., preprint.
79. Fisher J. E., in *Intercalculated Layer Materials,* pp. 481–532. D. Reidel, Dordrecht (1979).
80. Grabowski M. and Sham L. J., *Phys. Rev. B* **29,** 6132 (1984).
81. Miller B., Rosamilia J. M., Dabbagh G., Muller A. and Haddon R. C., preprint.
82. Allemand P. M., Khemani K. C., Koch A., Wudl F., Holczer K., Donovan S., Gruner G. and Thompson J. D., *Science* **253,** 301 (1991).